Journal of Nuclear Materials 400 (2010) 175–181

Contents lists available at ScienceDirect

Journal of Nuclear Materials

journal homepage: www.elsevier.com/locate/jnucmat

Review

Helium diffusion coefficient measurements in R7T7 nuclear glass by $^{3}He(d,\alpha)^{1}H$ nuclear reaction analysis

F. Chamssedine [a,*], T. Sauvage [a], S. Peuget [b], T. Fares [b], G. Martin [c]

[a] CEMHTI – Conditions Extrêmes et Matériaux: Haute Température et Irradiation, CNRS, 3A rue de la Férollerie, 45071 Orléans cedex 2, France
[b] CEA Marcoule, DEN/DTCD/SECM, BP 17171, 30207 Bagnols-sur-Cèze cedex, France
[c] CEA Cadarache, DEC/DEN/SESC/LLCC, 13108 St. Paul Lez Durance cedex, France

ARTICLE INFO

Article history:
Received 12 September 2008
Accepted 23 February 2010

ABSTRACT

The immobilization of fission products and minor actinides by vitrification is the reference process for industrial management of high-level radioactive wastes generated by spent fuel reprocessing. Radiation damage and radiogenic helium accumulation must be specifically studied to evaluate the effects of minor actinide alpha decay on the glass long-term behavior under repository conditions.

A specific experimental study was conducted for a comprehensive evaluation of the behavior of helium and its diffusion mechanisms in borosilicate nuclear waste glass. Helium production was simulated by external implantation with ^{3}He ions at a concentration (≈1 at.%) 30 times higher than obtained after 10,000 years of storage. Helium diffusion coefficients as a function of temperature were extracted from the depth profiles after annealing. The $^{3}He(d,\alpha)^{1}H$ nuclear reaction analysis (NRA) technique was successfully adopted for low-temperature in situ measurements of depth profiles. Its high depth resolution revealed helium mobility at temperatures as low as 253 K and the presence of a trapped helium fraction. The diffusion coefficients of un-trapped helium atoms follow an Arrhenius law between 253 K and 323 K. An activation energy of 0.55 ± 0.03 eV was determined, which is consistent with a process controlled by diffusion in the glass free volume.

Contents

1. Introduction

R7T7 borosilicate glass was selected to immobilize the high-level radioactive wastes arising from spent fuel reprocessing. Fission products and minor actinides vitrified in the nuclear glass generate

* Corresponding author. Tel.: +33 238 257 646; fax: +33 238 630 271.
E-mail address: fadel.chamssedine@cnrs-orleans.fr (F. Chamssedine).

0022-3115/$ - see front matter © 2010 Elsevier B.V. All rights reserved.
doi:10.1016/j.jnucmat.2010.02.023

self-irradiation by β, γ and α decay. The effects of radiation on the glassy matrix are one of the major points to be considered for a waste package performance assessment. The main source of radiation damage is α decay, because the number of atoms displaced by each α disintegration is much larger than that from the β and γ decay. Some studies carried out on nuclear borosilicate glasses have revealed variations in the glass density (slight swelling or densification depending on the chemical composition of the nuclear glass) and in the mechanical properties (Young's modulus, hardness, toughness) due to the accumulation of α decays within the glass [1–7]. These modifications have been attributed to the consequences of the nuclear interactions induced by the alpha decay recoil nuclei [5,7].

The behavior of the helium produced by the α-emitters present in the waste must be evaluated to determine the effect of helium generation on the glass integrity. This requires an assessment of helium diffusion in the glass to predict whether or not helium will be released from the glass matrix under disposal conditions.

To the best of our knowledge, three main techniques have been used to simulate helium accumulation induced by α decay in nuclear borosilicate glasses. The first consists in doping glass specimens with a short-lived actinide to obtain in a few years the cumulative dose received by the future glass packages over several millennia [4–8]. The second technique is based on irradiation of borosilicate glasses by thermal neutrons to generate a homogeneous helium concentration within the glassy matrix by the $^{10}B(n,\alpha)^{7}Li$ nuclear reaction [3,9]. Its high cross section value allows a high helium dose to be reached within a reasonable irradiation time. The helium permeation technique by hot isostatic pressing under helium atmosphere offers the advantage of introducing helium in the glassy matrix without damage [10].

In this study, the accumulation of helium in the glass was obtained by implanting ^{3}He ions. Although the implantation technique is easy to implement, it allows a high helium dose to be accumulated in only a few minutes. This technique produces a lower defect concentration than doping or $^{10}B(n,\alpha)^{7}Li$ techniques. However, prior to the helium implantation, the defect concentration can be enhanced by heavy ion irradiation in order to predict the influence of defects on helium diffusion. The analyses were performed in the DIADDHEM (DIspositif d'Analyse de la Diffusion du Deutérium ou de l'HÉlium dans les Matériaux) experimental facility. The $^{3}He(d,\alpha)^{1}H$ nuclear reaction analysis method (NRA) was used to determine the depth profile of the implanted helium concentration. The mechanisms involved in helium migration into borosilicate nuclear waste glass were investigated from the evolution of the concentration profiles as a function of the annealing conditions. The helium diffusion coefficients and activation energy in borosilicate glass were determined.

2. Experimental

2.1. DIADDHEM description

This experimental study was performed in the DIADDHEM facility developed at CEMHTI laboratory and installed on a Van de Graaff accelerator beamline. The originality of this facility resides in the coupling of the NRA coincidence technique with sample heating and cooling systems (Fig. 1). It offers the advantage of implanting helium at low-temperature and allowing in situ measurements of helium desorption or depth profiles over a wide range of annealing temperature from 120 K to 1170 K. The main components of this device are three particle detectors and a motorized goniometer (one rotation and two translation drives). The goniometer is equipped with an electronic bombardment furnace heating the rear side of the sample holder and a cooling system including

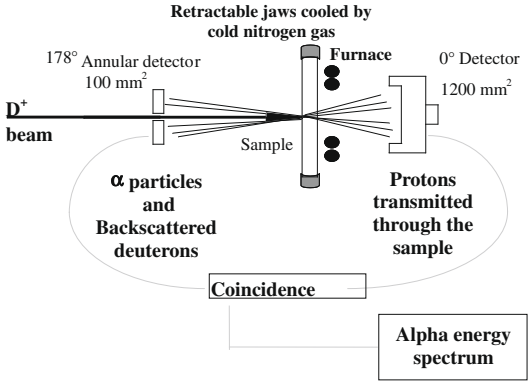

Fig. 1. Experimental configuration of DIADDHEM.

two retractable jaws cooled by cold nitrogen gas. The DIADDHEM facility was described in detail in a previous paper [11].

The $^{3}He(d,\alpha)^{1}H$ NRA technique is based on irradiating the sample by a deuteron beam produced by a 3 MV Van de Graaff accelerator. The detection in coincidence of both reaction products (α-particles and protons) emitted from the $^{3}He(d,\alpha)^{1}H$ nuclear reaction reduces the backscattered ^{2}H intensity by a factor of about 4×10^{4} and provides α-particle spectra free of spurious signals in the region of interest (Fig. 2). The helium depth profile is measured from the alpha energy spectrum at a depth of up to 6 μm into borosilicate glass. More details about the NRA coincidence technique are described by Sauvage et al. [12].

2.2. Sample preparation

Cylindrical borosilicate glass rods were fabricated at CEA Marcoule and cut into disks by the Primeverre in Montpellier. The chemical composition of the studied glass is indicated in Table

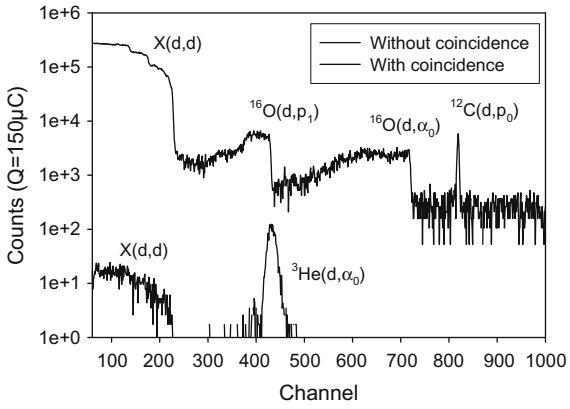

Fig. 2. Energy spectra in single and coincidence mode at 178° for borosilicate glass. Analysis was performed with 900 keV D^{+} ions at a charge of 150 μC.

Table 1
Chemical composition of the studied glass.

Component concentration (mol%)					
SiO_2	52.8	SrO	0.2	La_2O_3	0.2
B_2O_3	14.1	ZnO	2.2	Ce_2O_3	0.2
Al_2O_3	3.4	Fe_2O_3	1.3	Nd_2O_3	0.3
Na_2O	11.3	ZrO_2	1.5	Pr_2O_3	0.1
Li_2O	4.6	MoO_3	0.8	TeO_2	0.1
Cs_2O	0.3	MnO_2	0.3	P_2O_5	0.1
CaO	5.0	NiO	0.3	Y_2O_3	0.2
BaO	0.3	Cr_2O_3	0.2	Other oxides	0.2

1. The specimens were polished on both sides using 6 μm diamond paste and the surface of the analysis side was then finished using 1 μm diamond paste. The resulting disks were approximately 270 ± 20 μm thick and 8.8 mm in diameter. A carbon layer (~15 nm) was deposited on the analysis surface of the disks to avoid electrical discharge during the $^3He^+$ or D^+ bombardment and physical deterioration of the disk.

2.3. Helium implantation, annealing and determination of helium depth profiles

In a preliminary study, a borosilicate disk was implanted at room temperature with 600 keV ^{3}He ions at a dose of 5×10^{15} at cm^{-2}. Online measurement of the helium desorption revealed a 20% loss from the initial helium concentration after storage at room temperature for 20 h. These results highlight the strong mobility of helium at room temperature. Consequently, the helium implantation and the helium depth profile measurement must be performed at a lower temperature. A specific procedure was therefore defined for the study of helium in borosilicate glass in order to minimize helium diffusion during implantation and profiling (Fig. 3).

After cooling the sample to a temperature below 150 K, ^{3}He ions were implanted at an energy of 600 keV and a fluence of 2×10^{16} at cm^{-2} ($\sim 36 \times 10^{19}$ He g^{-1}). The as-implanted helium depth profile was then measured by maintaining the sample at that temperature. After sample thermal cycling, the sample was cooled again before determining the helium profile.

The helium depth profiles were measured using a 2×2 mm^2 deuteron beam at 900 keV. The depth profiles were extracted using the RESNRA (RESolution in NRA) freeware coupled to the SIMNRA 5.0 (simulation program for the analysis of NRA) software. This code allows the depth resolution as a function of the distance from the sample surface to be determined from the experimental alpha particle spectrum [13]. The depth resolution is 0.06 μm near the borosilicate glass surface and degrades with depth due to primary deuteron beam and alpha particle energy straggling [11].

Four temperatures were investigated. Samples S1, S2, S3 and S4 were annealed at 253 K, 273 K, 298 K and 323 K, respectively. The thermal cycle was carried out with positive and negative slopes of 15 K/min and 10 K/min, respectively.

3. Results and discussion

3.1. Helium depth profiles

^{3}He depth profiles of the samples before and after annealing are shown in Fig. 4. The maximum helium concentration $[He]_{max}$ of the as-implanted samples ranges from 1 to 1.15 at.% at a depth of 1.83 μm. The theoretical helium distribution determined by SRIM (Stopping and Range of Ions in Matter) calculations [14] is presented in Fig. 5. For a fluence of 2×10^{16} at cm^{-2}, the $[He]_{max}$ estimated by SRIM is 1.15 at.% at a depth of 1.9 μm. The maximum number of displacements per atom (dpa) is calculated as 0.68 within the nuclear cascade zone located at 1.83 μm. A difference of 0.07 μm is observed between the experimental and simulated helium distribution location. The depth resolution of the NRA coincidence technique (0.12 μm at 1.83 μm in borosilicate glass) is not sufficient to conclude that helium migration occurred within the nuclear cascade region during implantation [11].

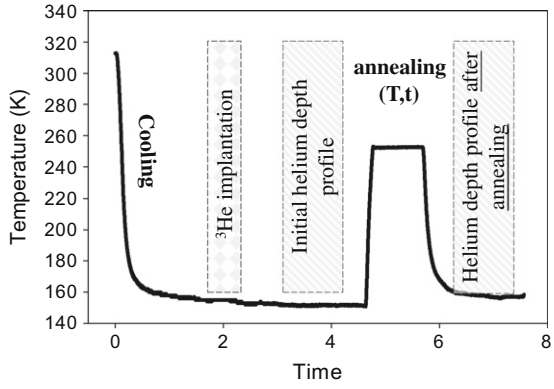

Fig. 3. Experimental procedure for ^{3}He implantation and depth profile determination before and after annealing stage.

The helium concentration depth profile broadens with the annealing temperature and time, due to helium diffusion within the glassy matrix. Helium mobility is observed at a temperature as low as 253 K (Fig. 4). From a temperature of 273 K, an asymmetry in the depth profiles appears to reveal anisotropy of the helium diffusion.

After annealing for 90 min at 298 K and for 10 min at 323 K, we observe a narrow peak located on the central region of the as-implanted profile and overlapping the broadened helium depth profile. This peak is a reliable indicator of the presence of a trapped helium fraction. This fraction is revealed in case of large diffusion of the un-trapped helium population. The helium profile of the sample annealed for 60 min at 323 K reveals thermal resolution of the trapped helium. Helium trapping may occur in defect clusters and/or in nanometer-size bubbles and/or porosities.

The total helium content of each profile was determined from the helium depth profile integration; no significant helium desorption was observed under all annealing conditions.

3.2. Helium diffusion coefficient calculation

3.2.1. Model calculation

A one-dimensional model used previously by Guilbert et al. [15] is applied to simulate the ^{3}He concentration profile changes after sample annealing.

$$\frac{\partial C_D(x,t)}{\partial t} = \frac{\partial}{\partial x}\left(D\frac{\partial}{\partial x}C_D(x,t)\right) \quad (1)$$

D is the diffusion coefficient at the annealing temperature T, x the distance from the sample surface and t the annealing time. The experimental results of depth profiling indicate trapping of a significant fraction of the initial implanted helium atoms. We then entered in the model a trapped helium population $C_T(x, 0)$ equal to a fraction λ of the initial helium distribution $C(x, 0)$. We assume that the trapped helium peak is located at the initial helium maximum concentration.

The helium concentration $C_D(x, 0)$ in Eq. (1) at annealing time $t = 0$ is considered as the fraction of helium diffusing in the borosilicate glass and corresponds to the term $(1 - \lambda) \cdot C(x, 0)$.

The final helium concentration profile $C(x, t)$ after an annealing time t is assumed to be the sum of the two contributions, one which can diffuse into the glass and another one which is trapped.

$$C(x,t) = C_D(x,t) + \lambda \cdot C(x,0) \quad (2)$$

This model does not directly take into account the mechanism of thermal resolution of helium during the annealing time t. The λ term is then estimated after each annealing stage.

The anisotropy of the helium profiles observed at temperatures above 273 K could indicate a space-dependence of the helium diffusion coefficient, as with glass damage. The effect of the glass damage on the helium diffusion mechanisms in borosilicate glasses is discussed in the literature. Malow and Andresen [9] observed a reduction of the apparent helium diffusion coefficients with

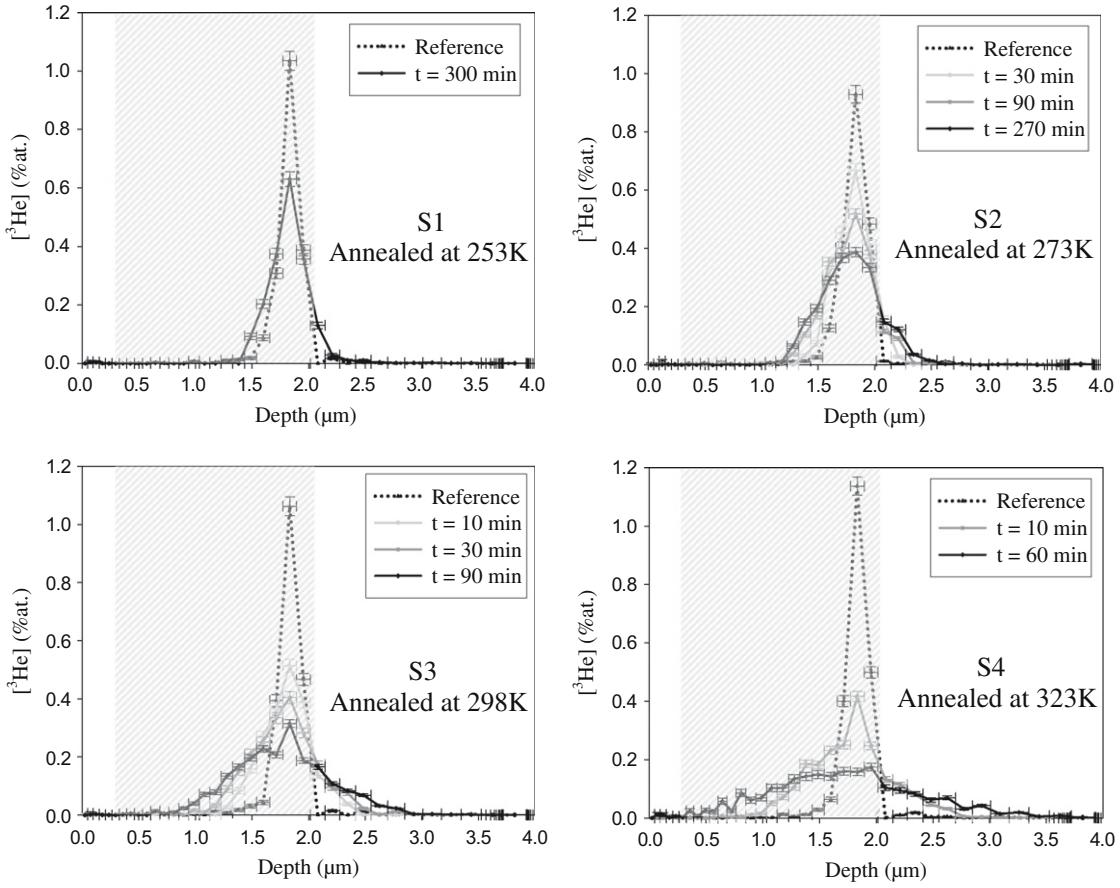

Fig. 4. Helium depth profiles of samples S1, S2, S3 and S4 implanted with 600 keV ^{3}He at 2×10^{16} ^{3}He cm^{-2}.

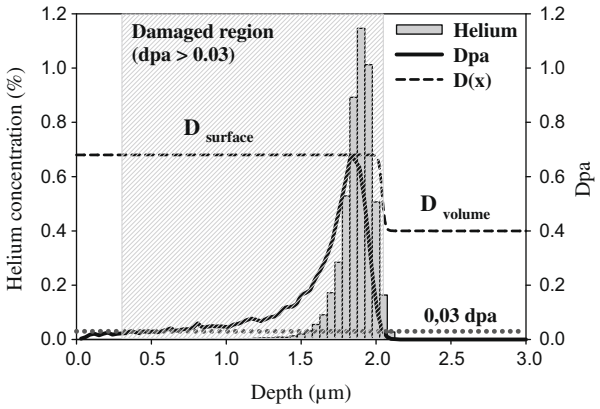

Fig. 5. Depth distributions of 600 keV ^{3}He$^+$ and of displacements yield per atom (dpa) calculated by SRIM at a fluence of 2×10^{16} at cm^{-2}. Spatial variation of $D(x)$ function introduced in the model calculation. The hatched zone on the graph represents the region damaged by ^{3}He implantation with a dpa value higher than 0.03 dpa.

increasing α dose generated by the ^{10}B(n,α)^{7}Li nuclear reaction. This change was attributed to the radiation damage of the glass. Peuget et al. [5] reported an impact of the alpha dose rate on the macroscopic and mechanical properties of R7T7 borosilicate glass doped with $^{244}CmO_2$. The authors described progressive swelling and a hardness reduction as a function of alpha decay doses for doses ranging from 10^{17} α/g to 2×10^{18} α/g (~0.083 dpa). No further significant variation was shown at higher doses, i.e. the glass swelling saturates at about 0.5% and the hardness decreases from the initial value by up to 30%. The authors ascribe the observed changes to the damage induced by nuclear interactions caused by recoil nuclei from alpha decays.

We have therefore introduced in our model a spatial dependence for D which reflects the presence of defects induced during the implantation stage. According to our implantation conditions (mono-energetic primary ^{3}He beam 600 keV ^{3}He$^+$, 2×10^{16} at cm^{-2}), the dpa profile simulated by SRIM is inhomogeneous (Fig. 5). The maximum number of dpa is estimated to be 0.68 and located at the depth of 1.83 μm. We assume that the glass is damaged when the variation of the macroscopic and mechanical properties determined by Peuget et al. [5] reaches half the saturation values. The corresponding α dose is then estimated at 7×10^{17} α/g, corresponding to 0.03 dpa. Hence, the layer of material for which the depth ranges from 0.30 μm to 2.04 μm is presumed damaged (Fig. 5). Because the experimental helium depth profiles (Fig. 4) reveal a very low helium concentration from the surface to the depth of 0.3 μm, the $D(x)$ function is simplified to two constants $D_{surface}$ and D_{volume} linked by the following expression:

$$D(x) = D_{surface} + \frac{(D_{volume} - D_{surface})}{2} \cdot \left(1 + \tanh\left[\frac{(x - x_D)}{\sigma_{D^2}}\right]\right) \qquad (3)$$

X_D is the maximum depth at which the material is considered damaged and σ_D the depth resolution of NRA coincidence technique at the depth of X_D. The simulation is performed with the $D(x)$ equation in which X_D and σ_D values are set at 2.04 μm and 0.14 μm, respectively. The 0.14 μm value of σ_D corresponds to the depth resolution at X_D of the depth profiling technique used.

3.2.2. Results of simulation

A set of calculations with $D_{surface}$, D_{volume} and λ as parameters was performed to achieve the best fit of each experimental helium

profile. The more pertinent depth profiles as function of the annealing stage and their simulation are compared in Fig. 6. The resulting $D_{surface}$, D_{volume} and λ values are reported in Table 2. The standard deviations are determined by iterative simulation with different D and λ couple parameters and calculation of the Pearson correlation coefficient.

All the profiles are correctly fitted. The fit is better for the lower temperature than for the higher ones where an imperfect simulation of the rising edge of the helium peak (Fig. 6b and c) is observed.

The simulation results show helium trapping and helium thermal resolution phenomena. With regard to the λ values determined for the shortest annealing time, the quantity of trapped helium after implantation at 130 K is estimated between 10% and 30% of the initial helium concentration. The trapping yield is determined more precisely in the case where the trapped helium population can be deconvoluted from the helium diffusing within the glassy matrix. The most pertinent initial trapped helium fraction is observed after annealing for 10 min at 323 K, i.e. 19% with an absolute standard deviation of 1% (Fig. 6c). This initial trapping fraction could be underestimated because of a possible helium thermal resolution during the time t_1 necessary to reach the annealing temperature and to return to 130 K, but it could not exceed 30% (see Table 2). The helium would be trapped from implantation-induced defects and diffused after thermal resolution in the free volumes of the glass. At 323 K, the trapped helium fraction decreases from 19% after 10 min of annealing to 3% after 60 min (Table 2), i.e. the thermal resolution of trapped helium is highly effective at this temperature.

Table 2
Helium diffusion coefficients D and trapped fraction λ calculated from the simulation of the change of helium depth profiles after annealing stages.

Sample annealed	$D_{surface}$ 10^{-14} cm^2 s^{-1}	D_{volume} 10^{-14} cm^2 s^{-1}	λ (%)
S1-253 K			
300 min	0.4 ± 0.08	0.4 ± 0.08	18 ± 7
S2-273 K			
30 min	4.0 ± 0.8	4.0 ± 0.8	
90 min	3.0 ± 0.5	3.0 ± 0.5	15 ± 5
270 min	1.7 ± 0.3	1.5 ± 0.3	5 ± 5
S3-298 K			
10 min	38 ± 8	30 ± 5	15 ± 5
30 min	22 ± 3	19 ± 1	10 ± 2
90 min	20 ± 2	15 ± 1	10 ± 2
S4-323 K			
10 min	125 ± 10	125 ± 10	19 ± 1
60 min	75 ± 5	70 ± 10	3 ± 1

The simulation results do not show a significant difference between $D_{surface}$ and D_{volume}. A slight decrease of $D_{surface}$ and D_{volume} with time is observed. Two plausible interpretations can be advanced. Firstly, D is estimated from the evolution of the helium depth profile after annealing versus the as-implanted profile as reference. Consequently, this estimation is made without taking into account the helium diffusion during the time t_1 necessary to reach the annealing temperature and to return to 130 K. This influence should be predominant for short annealing times. Because the rate of temperature variation is 15 K/min and 10 K/min for the positive

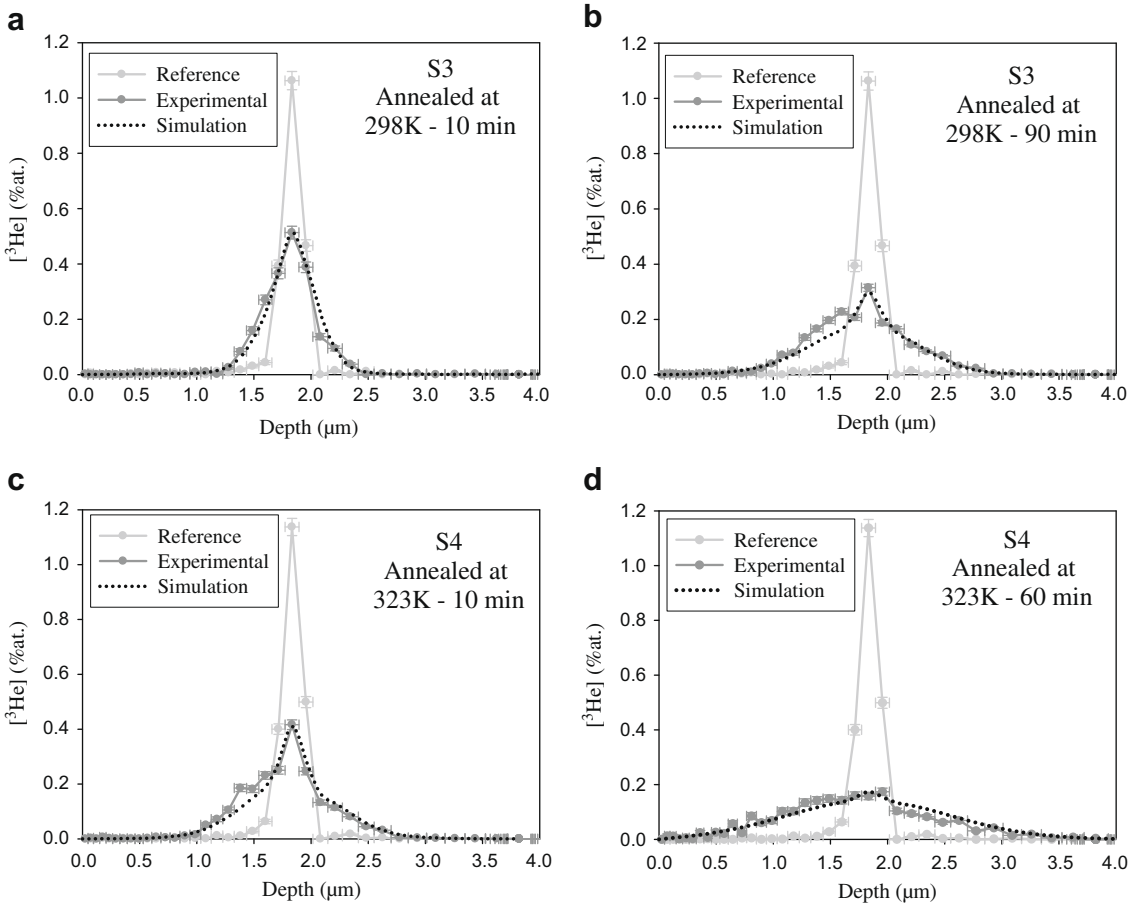

Fig. 6. Comparison between best-fit calculations and the corresponding experimental helium profiles obtained after annealing stage.

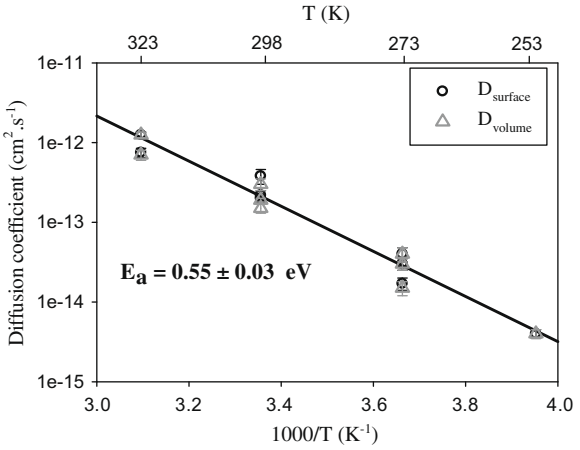

Fig. 7. Arrhenius plot of $D_{surface}$ and D_{volume} diffusion coefficients.

and negative slopes, this cannot explain the variation in D observed at 273 K for long annealing times. In any case, experimental helium depth profiles at 298 K and 323 K with an annealing time of 0 min will be measured to conclude on this point.

Secondly, the determination of the D values can be affected by helium resolution phenomenon. In case of a high helium resolution fraction, D values would be underestimated. This can explain an apparent decrease in the diffusion coefficient over time.

Because the simulation results reproduce the data quite well, differences in $D_{surface}$ and D_{volume} cannot lead to the slightly asymmetric profiles observed at 298 and 323 K. Another mechanism should be taken into account to better fit this asymmetry; it may be related to the resolution of trapped helium atoms in the damaged zone.

An upgrade of the simulation model is under development to take into account the trapped helium resolution kinetics.

3.3. Activation energy

The $D_{surface}$ and D_{volume} diffusion coefficients were plotted on a logarithmic scale versus the reciprocal Kelvin temperature (Fig. 7), resulting in straight lines with excellent Pearson's chi-square values, from which we estimated two values for the activation energy of helium diffusion. The difference between the two activation energy values for helium diffusion towards the surface (0.56 ± 0.02 eV) and the volume (0.55 ± 0.03 eV) is considered non-significant. The activation energy of helium diffusion in this glass is estimated at 0.55 ± 0.03 eV.

This activation energy is consistent with helium diffusion in the free volume of borosilicate glass systems. Because inert gases do not interact with the glass network, Doremus suggested that the gas atoms occupy empty interstices within the network [16]. The size of the interstitial space is directly related to the glass chemical composition, and changes the helium diffusion kinetics. The density and the size of the interstitial sites available for helium diffusion affect the doorways and the jump distance between the interstitial sites, which can modify the activation energy and/or the diffusion mechanism [17–20].

The glass studied in this work is a very complex borosilicate composition with numerous network formers (Si, B, Al, Fe), network modifiers (Na, Li, Ca, Sr, Ba, etc.) and other elements whose role in the glass structure is not well known and cannot be easily related to the glass free volume. Care must therefore be taken in comparing the activation energy measured in this study with the values observed on simpler borosilicate glasses. Nevertheless, Altemose [10] used the permeation technique to investigate helium diffusion between 460 and 800 K in simple borosilicate glasses with variable alkali content. The permeation technique introduces a homogenous helium concentration in volume without damage. The author noted an increase in the activation energy of helium diffusion as a function of the alkali concentration (Table 3). It varied from 0.22 eV for the glass with 1.94 mol% of Na_2O, which is close to the value measured on vitreous silica (0.26 eV [17,21]), to 0.45 eV for the glass with 11.9 mol% of Na_2O. The activation energy determined for the material studied in this work (11.3 mol% of Na_2O) is closer to the one corresponding to the highest Na_2O content (SiO_2: 69 mol%, B_2O_3: 16%, Al_2O_3: 1%, Na_2O: 11.9%) [10]. The high activation energy value we obtained could be related to the high concentration of alkali and alkali-earth atoms in the studied glass (Na_2O: 11.3 mol%, Ca_2O: 5%, BaO: 0.3%, SrO: 0.2%) (Table 1). Alkali and alkali-earth atoms certainly fill more the interstitial sites available for helium diffusion and maybe also increase the jump distance.

3.4. Effect of glass damage on helium diffusion

In Table 3 and Fig. 8, the obtained helium diffusion coefficients are compared with those reported in the literature using doping and the $^{10}B(n,\alpha)Li^7$ techniques [6,8,9]. The main differences of the implantation technique used in this study with these techniques are the heterogeneity of helium concentration in volume and the lower helium concentration to defect concentration ratio.

The helium depth distribution determined at 253 K, 273 K and 298 K (expect the profile obtained after annealing for 90 min at 298 K) broadens within an assumed damaged zone (hatched area in Fig. 4). Therefore, the corresponding diffusion coefficients $D_{surface}$ and D_{volume} are assumed to be determined in a damaged material. However, we attribute a lower reliability to the estimated

Table 3
Summary of our results and comparison with the literature data.

Author	Material	He incorporation mode	%[He]	dpa	D at 298 K (cm²/s)	Activation energy (eV)
Perkins and Begeal [21]	Silicon dioxide	Permeation	–	–	2×10^{-8}	0.23
Altemose [10]	Sodium borosilicate (1.94% Na_2O)	Permeation	–	–	3×10^{-8}	0.22
Altemose [10]	Sodium borosilicate (11.9% Na_2O)	Permeation	–	–	8×10^{-11}	0.45
Malow B [9]	Zinc borosilicate	$^{10}B(n,\alpha)^7Li$	0.0003	0.002	8×10^{-15}[a]	0.8
Turcotte [6]	Zinc borosilicate	^{244}Cm doping	0.002	0.034	2×10^{-14}[a]	0.65
Hall [8]	Borosilicate	^{238}Pu doping	0.0025	0.043	4×10^{-15}[a]	0.75
Malow A [9]	Zinc borosilicate	$^{10}B(n,\alpha)^7Li$	0.02	0.14	1×10^{-19}[a]	1.15
Malow C [9][a]	Zinc borosilicate	$^{10}B(n,\alpha)^7Li$	–	–	2×10^{-12}[a]	0.47
This study	R7T7	^3He implantation	Up to 1.15	0–0.68	2×10^{-13}	0.55

[*] Malow A, data obtained on a damaged glass (dpa = 0.14).
Malow B, data obtained on a low damaged glass (dpa = 0.02).
Malow C, extrapolated data obtained on restored damaged glasses by heat treatment at temperatures above 673 K; these samples can be considered as pristine glasses.
[a] Extrapolated value.

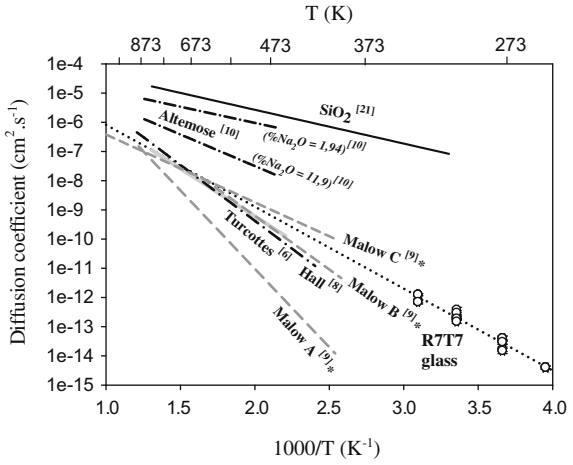

* Malow A, data obtained on a damaged glass (dpa=0.14)

Malow B, data obtained on a low damaged glass (dpa=0.02)

Malow C, extrapolated data obtained on restored damaged glasses by heat treatment at temperatures above 673 K; these samples can be considered as pristine glasses

Fig. 8. Helium diffusion coefficients versus reciprocal Kelvin temperature reported in the literature and obtained by the present study.

$D_{surface}$ values compared with the values for D_{volume} because of the imperfect simulation of the depth profile towards the surface.

A large diffusion towards the bulk in a region assumed to be undamaged material is observed after annealing at 298 K (for 90 min) and 323 K. These D_{volume} values can be related to helium diffusion within an undamaged material. As shown in Fig. 6d, the experimental depth profile obtained after annealing at 323 K for 60 min is correctly simulated towards the surface and the volume with the same diffusion coefficient.

We conclude that the damage yield induced by ^{3}He implantation at 2×10^{16} at cm^{-2} has no significant influence on the helium diffusion. More precisely, the heterogeneity of the damage distribution does not appear to affect helium diffusion. The $D_{surface}$ and D_{volume} diffusion coefficients follow an Arrhenius law with the same activation energy (Fig. 7).

The literature studies listed in Table 3 are based on helium release measurements by thermal desorption spectroscopy (TDS). Generally, TDS is a powerful tool for providing fast and reliable characterization of the helium diffusion mechanisms. In a glassy matrix, however, this technique gives an apparent diffusion coefficient combining thermal diffusion in free volumes and helium trapping/resolution phenomena. In contrast, NRA experimentally reveals the presence of helium trapping and resolution mechanisms. We can suspect therefore that the decrease in the apparent diffusion coefficient of helium observed by Malow and Andresen [9] could be due to the trapping effect induced throughout the damaged glass volume. To explain an apparent decrease in diffusivity with time, Turcotte proposed that the helium desorption could be first controlled by thermal diffusion and then by resolution effects. This could lead to errors in determining the helium diffusion coefficient [6].

Whatever the high damage yield (up to 0.68 dpa) induced by helium implantation within the nuclear cascade zone, the diffusion coefficients and activation energy of this study are in closer agreement with the ones determined on fresh or slightly damaged borosilicate glasses (Table 3).

In fact, as shown in Table 3, our activation energy (0.55 eV) and helium diffusion coefficient at room temperature (2×10^{-13} cm^2 s^{-1}) are close to the values (0.47 eV and 2×10^{-12} cm^2 s^{-1}) obtained by the ^{10}B(n,α)^{7}Li technique in a glass annealed at high temperature ($T > 773$ K), temperature range in which the glassy matrix has been restored by heating [9].

Some specific experiments on samples pre-irradiated by heavy ions are in progress to confirm the initial data on the impact of glass damage on the intrinsic helium diffusion coefficient.

4. Conclusion

The behavior of helium in nuclear borosilicate glass was investigated by helium-3 ion implantation. This method offers the possibility of accumulating a high helium dose in a short time. Helium diffusion in a glassy matrix is measured by NRA coincidence. Compared with the thermal desorption spectroscopy method used in the literature, NRA highlights the different mechanisms involved in the behavior of helium within the glass. This technique reveals the presence of a trapped helium fraction after implantation, estimated at about 20% of the initial helium fluence. Thermal resolution of the trapped helium was demonstrated depending on the annealing time and temperature. Helium diffusion coefficients in borosilicate glass were determined and the results do not reveal a significant effect of the glass implantation damage on the helium diffusion coefficients. The activation energy of helium diffusion within this borosilicate glass was estimated at 0.55 ± 0.03 eV. This study proves that the helium ion implantation is a suitable technique to better understand helium behavior in nuclear glass.

Acknowledgments

This study was carried out under a research program funded jointly by CNRS-CEMHTI, CEA, GDR MATINEX and AREVA NC.

References

[1] W.J. Weber, F.P. Roberts, Nucl. Technol. 60 (1983) 178.
[2] W.J. Weber, R.C. Ewing, C.A. Angell, G.W. Arnold, A.N. Cormack, J.M. Delaye, D.L. Griscom, L.W. Hobbs, A. Navrotsky, D.L. Price, A.M. Stoneham, M.C. Weinberg, J. Mater. Res. 12 (8) (1997) 1946.
[3] S. Sato, H. Furuya, T. Kozaka, Y. Inagaki, T. Tamai, J. Nucl. Mater. 152 (1988) 265.
[4] Y. Inagaki, H. Furuya, K. Idemitsu, T. Banba, S. Matsumoto, S. Murakoa, Mater. Res. Soc. Symp. Proc. 257 (1992) 199.
[5] S. Peuget, J.N. Cachia, C. Jégou, X. Deschanels, D. Roudil, V. Broudic, J.M. Delaye, J.M. Bart, J. Nucl. Mater. 354 (2006) 1.
[6] R.P. Turcotte, Ceramics and Graphite Section – Materials Department, Pacific Northwest Laboratories, Richland, Washington, Rapport BNWL-2051, 1976.
[7] S. Peuget, P.Y. Noel, J. L Loubet, S. Pavan, P. Nivet, A. Chenet, Nucl. Instrum. Methods Phys. Res. B 246 (2006) 379.
[8] A.R. Hall Weldrick, Chemistry Division, AERE Harwell, Rapport AERE-R 8706, 1977.
[9] G. Malow, H. Andresen, in: G.J. McCarthy (Ed.), Scientific Basis for Nuclear Waste Management, vol. 1, 1979, p. 109.
[10] V.O. Altemose, J. Am. Ceram. Soc. 56 (1) (1973) 1.
[11] F. Chamssedine, T. Sauvage, S. Peuget, Nucl. Instrum. Methods Phys. Res. B, in press. Accepted manuscript, Available online 25 February 2010.
[12] T. Sauvage, H. Erramli, S. Guilbert, L. Vincent, M.-F. Barthe, P. Desgardin, G. Blondiaux, C. Corbel, J.P. Piron, F. Labohm, A. Van Veen, J. Nucl. Mater. 327 (2004) 159.
[13] G. Martin, T. Sauvage, P. Desgardin, P. Garcia, G. Carlot, M.F. Barthe, Nucl. Instrum. Methods Phys. Res. B 258 (2007) 471.
[14] J.F. Ziegler, J.P. Biersack, U. Littmark, The Stopping and Range of Ions in Solids, vol. 1, Pergamon Press, 1985.
[15] S. Guilbert, T. Sauvage, P. Garcia, G. Carlot, M.-F. Barthe, P. Desgardin, G. Blondiaux, C. Corbel, J.P. Piron, J.-M. Gras, J. Nucl. Mater. 327 (2004) 88.
[16] R.H. Doremus, J. Am. Ceram. Soc. 49 (9) (1966) 461.
[17] J.F. Shackelford, B.D. Brown, J. Am. Ceram. Soc. 63 (9–10) (1980) 562.
[18] J.F. Shackelford, J. Non-Cryst. Solids 253 (1999) 231.
[19] C. Tournour, J.E. Shelby, J. Non-Cryst. Solids 349 (2004) 209.
[20] J.C. Lapp, J.E. Shelby, Phys. Chem. Glasses 38 (5) (1997) 256.
[21] W.G. Perkins, D.R. Begeal, J. Chem. Phys. 54 (4) (1971) 1683.